ISSN 2616-5767 Vol.6, Issue 6: 58-64, DOI: 10.25236/AJETS.2023.060609

Application of Multimedia Virtual Technology in Mechanical Engineering Display Design

Yihui Chen

Tangshan Polytechnic College, Tangshan, 063299, China

Abstract: *Virtualization technology is one of the high and new technologies nowadays, and it is extremely important for the design of application products and mechanical objects. This provides a good design platform and development space for designers of application products and mechanical structures, more clearly and intuitively, it shows a self-virtualized simulation scene of people's future virtual products and mechanical engineering models, unknown virtual products and mechanical engineering models, ideal virtual products and mechanical engineering models or all real things that people imagine creating and show. The interaction between mobile virtual and reality is constantly developed and respected, and the man-machine interaction operation mode is realized. This paper introduces the system dynamics formula of the barge system in the upper block on the offshore electric platform and the calculation of acceleration and inertia force in its inertial load. In the virtual system, the dynamic model is used to calculate the kinetic energy and potential energy of mechanical engineering, and the algorithm model is applied to the angle and acceleration of joints on the robot. Three kinds of network models are simplified by simplification algorithm, and the models are compared in two aspects of visual geometry error and visual error. Finally, the video quality is reacted by different users, and the model performance is compared.*

Keywords: *mechanical engineering, virtual technology, vision, video quality*

1. Introduction

In biology, the development of improved early diagnosis strategies and treatment schemes for many rare diseases can utilize the defects of strengthening bioenergy and protein quality control system related to disease specificity and strengthen the imbalance of cytoskeleton tissue in the pathogenesis of ARSACS [1]. In case of fire, the two-way reinforced concrete slab is destroyed and collapsed by flame, so the fire resistance test of the two-way slab with three simple supporting edges and one clamping edge is carried out, and the formula for calculating its ultimate bearing capacity is obtained [2]. The individual minimum and global minimum in limit equilibrium method are used to estimate the bearing capacity, The failure mechanism of determining bearing capacity and the critical failure mechanism of resistance caused by cohesion and soil weight are defined from α and β angles respectively, and a clear single failure mechanism is obtained to estimate the total bearing capacity, and the results are compared with those of finite element analysis [3]. In the upper line limit theorem, the two-dimensional sliding failure mechanism of rigid block system with network is constructed, and the ultimate bearing capacity of rough foundation is analyzed [4]. It is very difficult and complicated to calculate the ultimate bearing capacity of single pile. The contact element method is used to calculate 343 different ultimate bearing capacity of single pile. In practical engineering, simple calculation formula, empirical formula in code, contact element method and static load experiment method are used to calculate the ultimate bearing capacity of single pile to test the simple calculation formula [5]. Because offshore wind power platforms are vulnerable to sudden extreme loads such as earthquakes and high current loads. The top-heavy structure in offshore wind farm makes it more dangerous. The effects of wet and dry environment, earthquake excitation mode, whipping effect and weak position of electric platform structure are analyzed. The results show that the average damping rates of the first-order mode of water platform and non-water platform are 5.73% and 8.68%, respectively [6]. As soon as shape design parameters are used in the crankshaft port of the secondary development platform, the crankshaft can be parameterized. The final results show that this method can quickly generate the crank shape, thus reducing repeated operations and saving costs [7]. The three-dimensional problem is simplified to two-dimensional problem by comparing the solution with the three-dimensional formula in LIRA-SAPR software package and the experimental data of A.L. Krishan and A.I. Sagadatov [8]. Reinforced bending concrete structures by adding sections and evaluating the bearing capacity of

ISSN 2616-5767 Vol.6, Issue 6: 58-64, DOI: 10.25236/AJETS.2023.060609

these members with inclined sections is an urgent problem. By analyzing and developing theoretical calculations of reinforced concrete members inclined to the longitudinal axis, we can determine many areas, and the main methods are based on the calculation of material resistance foundation and the use of experience dependence [9]. The discontinuous layout optimization is applied to obtain the bearing capacity of rock mass in shallow ground. The numerical and analytical results based on sensitivity research are analyzed, which changes the three parameters of rock mass characteristics (rock type, uniaxial compressive strength and geological strength index), and shows that the nonlinear failure criterion needs to be fully linearized in numerical calculation [10]. Because of the complex geological conditions and many influencing factors in lava area, the experimental analysis of bridge engineering in karst area is carried out, and the calculation algorithm of vertical capacity of rock jacket pile in karst area by load transfer method is established [11]. The pollution load of plain river network is difficult to control, so a multi-objective system with multiple constraints is proposed, and the corresponding one-dimensional and 0-d models are established to calculate the load capacity [12]. Tower foundations in transmission line projects in western China are often affected by extreme weather. Using Bala fracture plane hypothesis and limit equilibrium method, a simplified calculation method for lifting bearing capacity of rock-socketed foundation piles is derived, and its reliability is verified [13]. The bearing capacity of reinforced concrete structure is very important, so the theoretical calculation of bearing capacity of concrete structure makes the development trend of reinforced concrete at home and abroad better and better [14].

2. Virtual technology theory

2.1 Barge System

The overall system dynamics formula of the barge of the upper block of the offshore electrical platform is as follows:

$$[M + A(\infty)]\ddot{x}(\tau) + \int_0^t K(t-\tau)\dot{x}(\tau)d\tau + Cx(t) = f_{exc} \tag{1}$$

Where M and C are the mass matrix of the upper block of the offshore electric platform and the restoring force matrix of the barge system in still water, τ is the time integration step, f_{exc} is the load, and $\ddot{x}(\tau)$, $\dot{x}(\tau)$ and $x(t)$ are the acceleration, velocity and displacement of the barge system, respectively.

Generally, the structural response under unit amplitude is used to evaluate whether the structure avoids the main frequency of waves on the sea surface. The dynamic equation of floating body in frequency domain is as follows:

The structural response under unit wave amplitude is generally used to evaluate whether the structure avoids the main frequency of the wave. The dynamic equation of the floating body in frequency domain is as follows:

$$R(\omega) = \frac{\overline{F_{exc}}(\omega)}{-\omega^2(M+A(\omega))+j\omega B(\omega)+C} \tag{2}$$

Where $\overline{F_{exc}}(\omega)$ is the unit amplitude.

The response spectrum of barge motion in the upper block under the action of random waves on the sea surface is as follows:

$$X(\omega) = S(\omega)|R(\omega)|^2 \tag{3}$$

$S(\omega)$ is the random wave spectrum, and $X(\omega)$ is the derivative of the acceleration and velocity response.

2.2 Inertial load

The acceleration and inertia force of the upper block are shown in Figure 1. Any point of the barge system block with mass *m* is determined by the inertia force generated by acceleration:

Newton's second law:

$$F_a = -ma \tag{4}$$

The tangential force and normal force of the upper block after rotation are as follows:

ISSN 2616-5767 Vol.6, Issue 6: 58-64, DOI: 10.25236/AJETS.2023.060609

$$F_\theta = -m(r\ddot{\theta}) \tag{5}$$

$$F_\omega = -m(rw_r^2) \tag{6}$$

Where ω_r and $\ddot{\theta}$ are the angular velocity and acceleration of the center of revolution of the whole barge system structure, respectively, and *r* is the radius of rotation.

Suppose the total inertial force F_y caused by rotation, translation and rotation about the Y axis:

$$F_y = -m(a_y + r\ddot{\theta}\sin\alpha + rw_r^2\cos\alpha) \tag{7}$$

Where a_y is the acceleration of translational acceleration in the y direction.

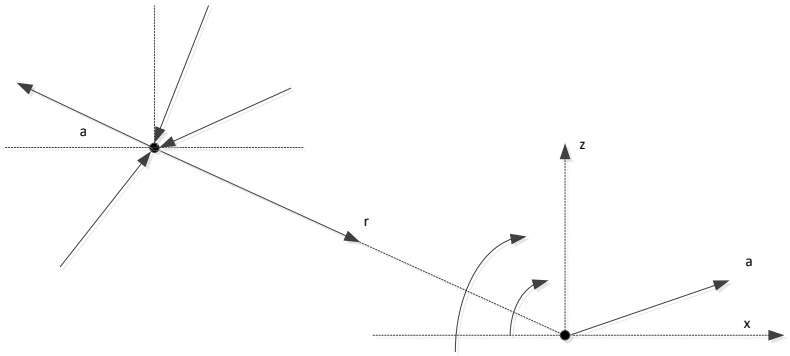

Figure 1: Schematic diagram of acceleration and inertia force

The combination of the upper block of offshore electric platform and inertial forces in different directions has five different normative inertial motions: rolling, pitching, swinging, heaving and heaving.

3. Virtual System

The essence of robot system is a mechanical system. The meaning of each variable of robot system is obtained, and the relationship between moment and trajectory is described by using the basic derivation thinking of dynamics.

Using Lagrange function, the coordinates $q_i(\theta_1, \theta_2, \theta_3, \theta_4, \theta_5, \theta_6)$ are selected

Function can be defined as:

$$L = T - u \tag{8}$$

According to the function, the expression of Lagrange equation is defined:

$$\frac{d}{dt}\frac{\partial L}{\partial \dot{q}_\iota} - \frac{\partial L}{\partial q_i} = \varepsilon_i \tag{9}$$

The matrix form obtained by the variant is defined:

$$\frac{d}{dt}\left(\frac{\partial L}{\partial \dot{q}_\iota}\right)^T - \left(\frac{\partial L}{\partial q}\right)^T = \varepsilon \tag{10}$$

In the above formula, $\dot{q}_\iota$ depends on the angular velocity of the joint, and ε depends on the joint torque, friction torque and torque caused by the actuator.

Create a virtual model, track and calculate the robot's motion trajectory in the world coordinate system, and get the synthesis of line-of-sight speed, running speed and driver's line-of-sight speed in the virtual scene. In the process of virtual simulation, the final picture is interfered by many factors, such as the turning speed, rotation angle and rotation direction of the robot. The virtual technology control chart is shown in Figure 2:

ISSN 2616-5767 Vol.6, Issue 6: 58-64, DOI: 10.25236/AJETS.2023.060609

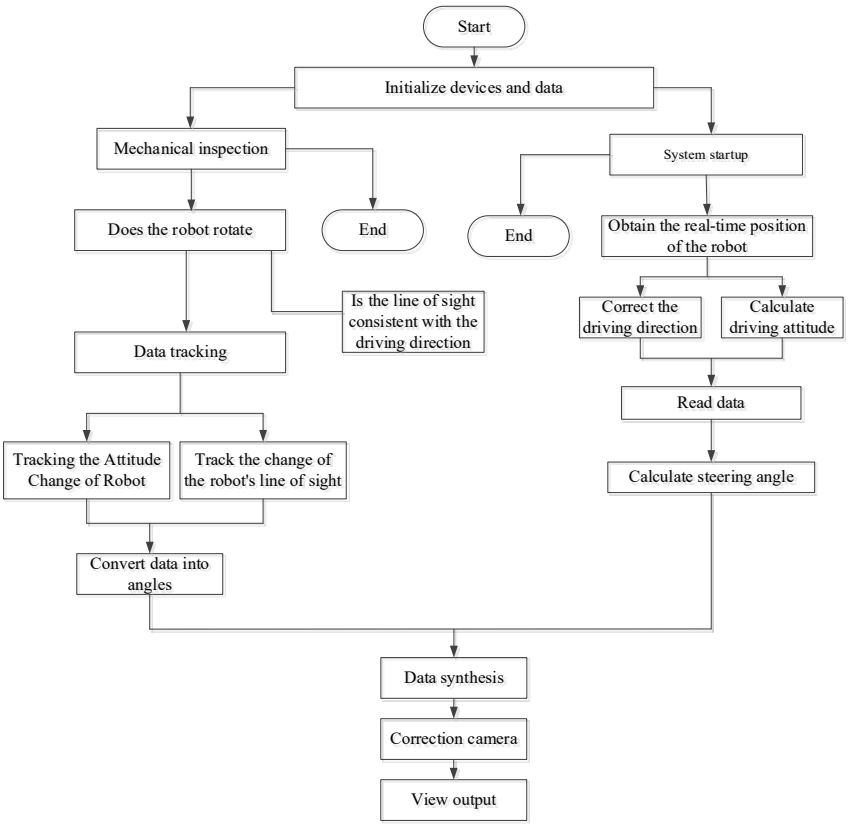

Figure 2: Control Chart of Virtual Technology

4. Experimental results and analysis

4.1 Complexity analysis of the model

In order to verify the reliability of the simplified algorithm combining visual perception with real geometric error in virtual technology, the simplified algorithm is implemented in programming language based on programming environment. The hardware environment is i7 processor, 3.4 GHz, 4GB memory, NVIDIA GeForce GTX 260 graphics card and 1GB video memory.

Three kinds of network models, Bunny, Armadillo and Dragon, which are common in the field of graph imaging, are used to compare the algorithms and analyze their reliability. The experimental network model puts the element information of the number of vertices and triangle patches of geometry and the number of vertices as shown in Table 1:

Table 1: Geometric Elements of Experimental Model

Model	Number of vertices	Number of triangular patches
Bunny	10058	19520
Armadillo	29100	63700
Dragon	43600	87100

It can be seen from Table 1 that Bunny model has the least number of vertices and triangle patches, which shows that the geometry complexity of the tested model is not high. The number of vertices and triangle patches in Dragon model is the most, which shows that the geometric complexity of the model is the highest. The higher the geometric complexity of the tested model, the more observation viewpoints are needed to perceive the model.

4.2 Model comparison

Qslim simplification algorithm, VMI simplification algorithm and Pooling simplification algorithm are used to simplify the images of three kinds of network models respectively, so as to minimize the difference in visual perception effect of the models. In order to get the comparison results of the advantages and disadvantages of the three simplified algorithms, the algorithm indexes of geometric

ISSN 2616-5767 Vol.6, Issue 6: 58-64, DOI: 10.25236/AJETS.2023.060609

average error and visual average error of these three models are evaluated and compared, as shown in Figures 3-5:

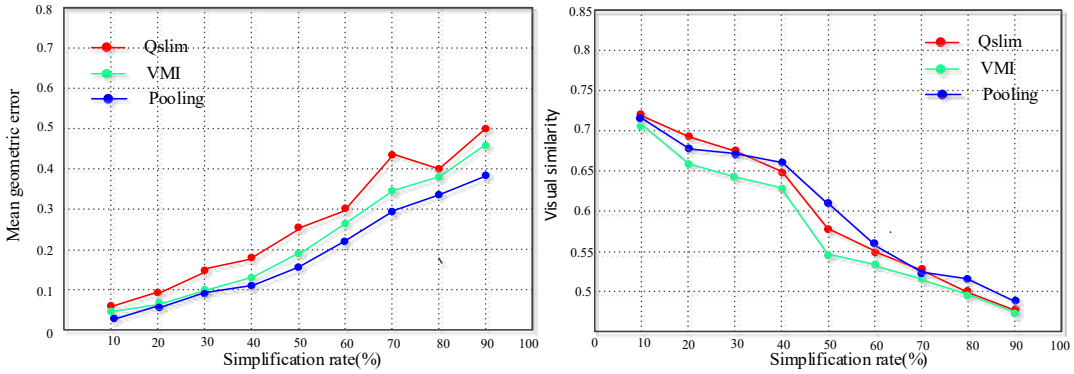

Figure 3: Three simplified algorithms of Bunny model

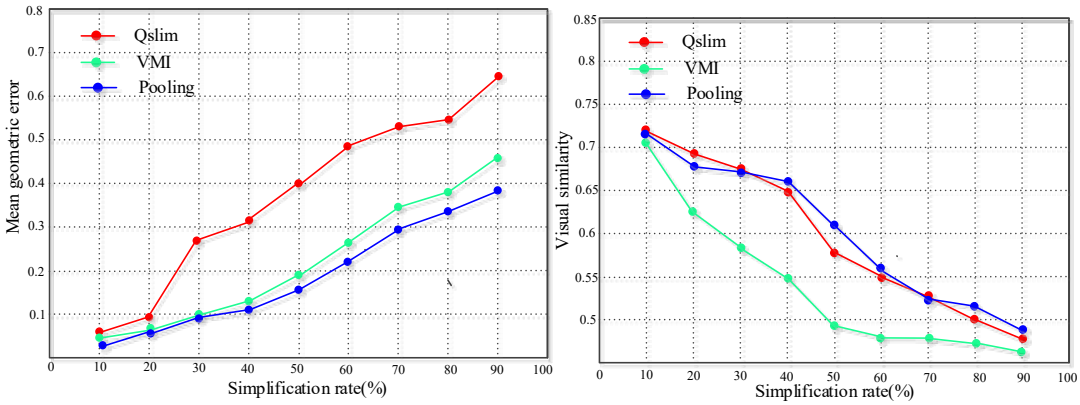

Figure 4: Three simplified algorithms of Armadillo model

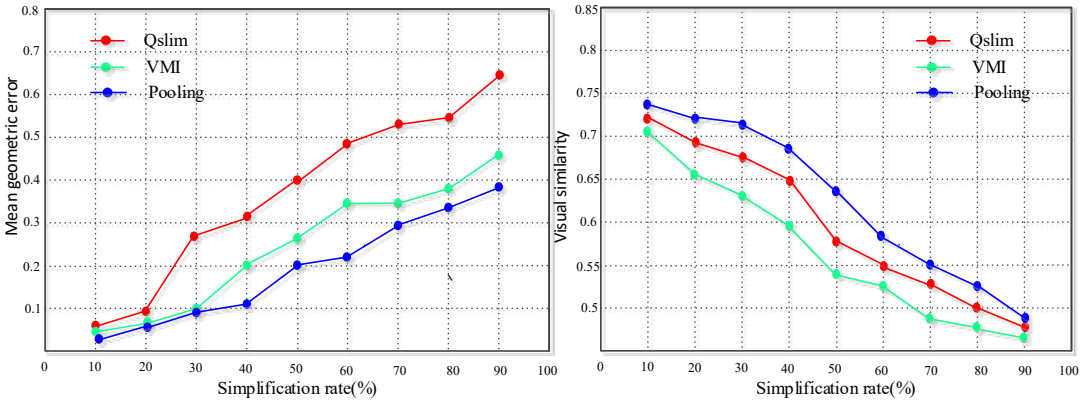

Figure 5: Three simplified algorithms of Dragon model

Figures 3-5 shows the comparison of geometric errors and visual similarity of Qslim simplification algorithm, VMI simplification algorithm and pooling simplification algorithm.

In order to further compare the simplification effect of the three simplification algorithms on the network model and the performance of the three simplification algorithms, the data are shown in Table 2:

Table 2: Performance comparison of three simplified algorithms

Error parameter	Bunny			Armadillo			Dragon		
	Q (%)	V (%)	P (%)	Q (%)	V (%)	P (%)	Q (%)	V (%)	P (%)
Geometric error	+15	+28	+36	+20	+31	+40	+21	+35	+44
Visual error	+18	+25	+40	+16	+26	+42	+15	+28	+43

ISSN 2616-5767 Vol.6, Issue 6: 58-64, DOI: 10.25236/AJETS.2023.060609

4.3 Simulation application

The experimental application simplification algorithm is used to simplify three kinds of network models for graphic presentation and video transmission. In the simulation scenario, the video is transmitted to multiple users through the traditional wireless network mode, and the video quality obtained by users A, B and C is compared to get which network model has better application effect and better performance, as shown in Figures 6-8:

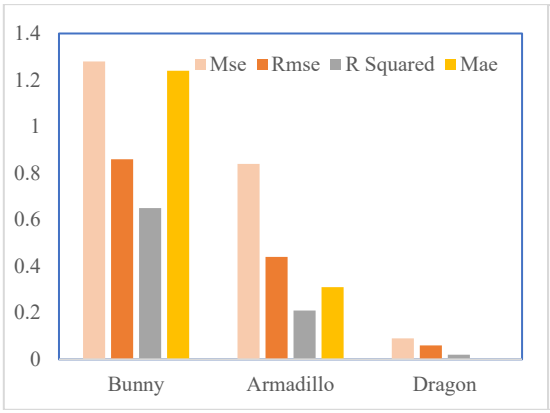

Figure 6: Video quality of user A

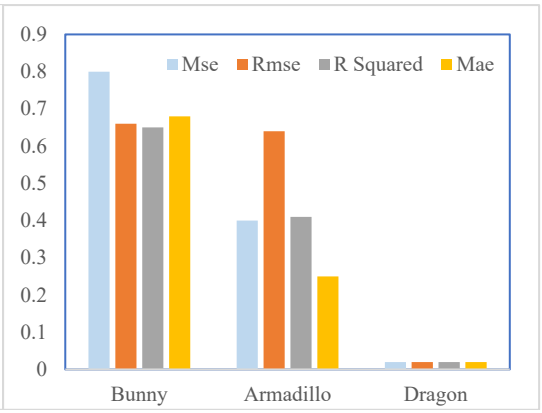

Figure 7: Video quality of user B

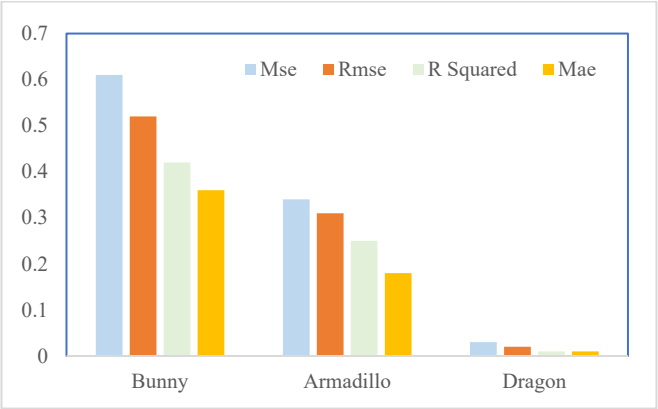

Figure 8: Video quality of user C

Figure 6-8 shows the comparison of the mean square error performance of the video quality obtained by users A, B and C. For the video quality obtained by three users, Bunny model has the highest performance value and the worst model performance, while Dragon model has the closest performance value to 0 and the best model performance.

5. Conclusion

Mechanical engineering combined with virtual technology to establish a dynamic model, using Bunny, Armadillo, Dragon three types of network model to simplify the visual error and visual error comparison, the simplified algorithm for comparative analysis. Mechanical engineering combined with multimedia technology draws the following conclusions:

(1) Different users compare the video quality of three different models, and the Dragon model has the best performance, and the equivalent values of mse, rmse, R squared and mae are close to 0.

(2) Three kinds of network models are simplified by using Qslim simplification algorithm, VMI simplification algorithm and pooling simplification algorithm. By comparison, the visual error and visual error of Dragon model are the smallest

(3) The dynamic model of mechanical engineering is established, and the formulas for calculating kinetic energy and potential energy and the kinetic energy expression of robot in a certain attitude are obtained.

ISSN 2616-5767 Vol.6, Issue 6: 58-64, DOI: 10.25236/AJETS.2023.060609

(4) Virtual design can combine real-time and live simulation technologies of virtual mechanical products, mobilize people's visual and tactile senses, and improve the accuracy of products.

(5) Virtual system can design virtual products, and finally get the real expectation of the products, and get different modes of virtual things and environment scenes.

References

[1] Morani Federica. Integrative Organelle-Based Functional Proteomics: In Silico Prediction of Impaired Functional Annotations in SACS KO Cell Model. [J]. Biomolecules, 2022, 12(8)
[2] Zhu Sanfan. Limit Carrying Capacity Calculation of Two-Way Slabs with Three Simply Supported Edges and One Clamped Edge under Fire [J]. Applied Sciences, 2022, 12(3): 1561-1561.
[3] Chuantao Chen and Mingzhong Gao and Ao Zhang. New Calculating Approach for the Ultimate Bearing Capacity of a Shallow Foundation [J]. International Journal of Geomechanics, 2020, 20(6).
[4] Lianheng Zhao and Feng Yang. Construction of improved rigid blocks failure mechanism for ultimate bearing capacity calculation based on slip-line field theory[J]. Journal of Central South University, 2013, 20(4): 1047-1057.
[5] Yaoze Liang, Jian Zhen, Baiguo Liang. Study and Application on Computational Methods for Ultimate Bearing Capacity of Single Pile [J]. Key Engineering Materials, 2008, 400-402(400-402): 329-334.
[6] Zhenzhou Sun et al. Experimental Analysis on Dynamic Responses of an Electrical Platform for an Offshore Wind Farm under Earthquake Load [J]. Journal of Marine Science and Engineering, 2019, 7(8): 279-279.
[7] Honggang Yang and Shujie Wang and Yirong Xie. Parametric Design of Crankshaft Based on CATIA Secondary Development Platform [J]. Applied Mechanics and Materials, 2014, 3365(602-605): 287-290.
[8] Chepurnenko Anton et al. Simplified 2D Finite Element Model for Calculation of the Bearing Capacity of Eccentrically Compressed Concrete-Filled Steel Tubular Columns[J]. Applied Sciences, 2021, 11(24): 11645-11645.
[9] Mazurak Andrii et al. Methods of Calculation the Increased Reinforced Concrete Elements by Carrying Capacity of Slope Sections [J]. IOP Conference Series: Materials Science and Engineering, 2021, 1203(2)
[10] Millán Miguel Angel and Galindo Rubén and Alencar Ana. Application of discontinuity layout optimization method to bearing capacity of shallow foundations on rock masses [J]. ZAMM - Journal of Applied Mathematics and Mechanics / Zeitschrift für Angewandte Mathematik und Mechanik, 2021, 101(10).
[11] He Qinghua et al. Algorithm for Vertical Bearing Capacity Calculation of Rock-Socketed Piles in Karst Area Based on Load Transfer Method[J]. IOP Conference Series: Earth and Environmental Science, 2021, 719(4)
[12] Xiao Wang and Min Pang and Mingzhi Zhao. Pollution Load Capacity Calculation Study Based on Multi-objective System in Trans-boundary Area, Plain River Network[J]. Bulletin of Environmental Contamination and Toxicology, 2021, 106(4): 1-8.
[13] Qinke Wang. Calculation method and influencing factors of uplift bearing capacity of rock-socketed pedestal pile[J]. Arabian Journal of Geosciences, 2021, 14(4): 1-15.
[14] Shkurupiy A A. Theoretical basis of bearing capacity calculation of the statically indeterminate reinforced concrete beams and its experimental research[J]. IOP Conference Series: Materials Science and Engineering, 2021, 1021(1).